Factorial Optimization of the Effects of Extrusion Temperature Profile and Polymer Grade on As-Spun Aliphatic–Aromatic Copolyester Fibers. I. Birefringence and Overall Orientation

Basel Younes,[1] Alex Fotheringham,[1] Hassan M. El-Dessouky[2,3]

[1]*School of Textiles and Design, Heriot-Watt University, Scottish Borders Campus, Netherdale, Galashiels TD1 3HF, United Kingdom*
[2]*Fibers Research Lab, School of Design, University of Leeds, Leeds LS2 9JT, United Kingdom*
[3]*Physics Department, Faculty of Science, Mansoura University, Egypt*

Received 19 October 2009; accepted 16 December 2009
DOI 10.1002/app.32002
Published online 3 June 2010 in Wiley InterScience (www.interscience.wiley.com).

ABSTRACT: The modeling of the relationship between the extrusion temperature profile and the polymer grade as well as the overall orientation of as-spun aliphatic–aromatic copolyester (AAC) fibers has been proposed. Depending on rheological results, AAC fibers were spun. In terms of the extrusion temperature profile and polymer grade, an appropriate statistical analysis of the optical anisotropy of the as-spun fibers was carried out. For measuring the fiber birefringence (optical anisotropy), an interferometric technique was employed. The interest of factorial design is in the restricted numbers of runs, 16 runs for a factorial design at 2 levels with 4 factors, and in the description of rheological mechanisms through mathematical interactions. The results obtained from the melt flow indexer give an explanation for the character of rheological properties and surface shape at different temperatures and loads at which recent analysis was performed. The overall orientation of the spun filaments has been modeled. The model allows a fast simulation to describe the behavior of factors-response relationship. © 2010 Wiley Periodicals, Inc. J Appl Polym Sci 118: 1270–1277, 2010

Key words: copolyester fibers; melt-spinning; temperature; birefringence; orientation; rheology

INTRODUCTION

Reducing, Reusing and Recycling of synthetic polymers has been studied to lower operation costs and to solve environmental waste problems, environmental pollution and the harming of wildlife.[1] Many articles have been published to produce and develop new biodegradable polymers.[2–6] As the use of composite materials is increasing, the replacement of chemical fibers with environmentally friendly fibers is a major interest of the textile industries.[7] The biopolymers are mainly based on starch, sugar, cellulose, or synthetic materials. Among petroleum based bio-polymers and by combining the biodegradability of aliphatic units with the aromatic one of good physical properties, great interest has been given on aliphatic and aromatic copolymers.[8] Compared to aliphatic polyesters, the aromatic form is often based on terephthalic diacid.[9,10] A number of aliphatic–aromatic copolyesters have been developed during the last decade to produce products with comparable cost to other plastic polymers and excellent properties.[11,12]

A number of researchers have tried to increase the strength of bio-plastics and their properties without affecting their biodegradability. A balance between the improvement of mechanical properties and the biodegradability needs to be investigated.[13] Aliphatic–aromatic copolyesters are potential candidates to make staple fibers for various nonwoven materials particularly for expendable uses in medicine and agriculture.[14–18] To improve biodegradable polyester properties, researchers have made crimp staple fibers from polylactic acid, thermoplastic starch, polycaprolactones and natural fibers. Other biodegradable products include disposable wipes, seed mats and erosion control items.

Extrusion temperature profile affects the properties, productivity and product cost.[19,20] As the viscoelastic nature of polymeric fluids has many complex effects on the flow stability,[21] molecular mobility and dye-ability is reduced by high orientation,[22,23] which appears as parallelization and extension of macromolecules and other structural units along the

Correspondence to: A. Fotheringham (a.f.fotheringham@hw.ac.uk).

fiber axis, affects physical properties and controls the fiber formation. The molecular orientation of fiber during spinning (i.e. draw-down ratio) is small as compared with that produced during post drawing (solid state draw ratio).[24,25]

To understand the viscoelastic behavior of the polymer, rheological study has to be considered. Melt flow index (MFI) is one of the most important properties for the quality control of polymers, the higher MFI, the lower resin velocity and molecular weight.[26]

Pre-experimental work has been done to find out the rheological data for determining the enhanced melt spinning conditions. This is to understand the viscoelastic and morphological properties of the aliphatic–aromatic copolyester (AAC). As-spun AAC fibers made of two different grades were spun at different extrusion temperature profiles. Some aspects of the modeling of melt spinning process for the manufacturing of AAC fibers were dealt with. The effects of the studied factors on the optical birefringence and the overall thermal behavior of the AAC fibers were presented. Accordingly the overall orientation of these fibers was modeled. Other properties of the AAC fibers will be reported in further work.

EXPERIMENTAL WORK

Material

A fully biodegradable petroleum aromatic-aliphatic copolyester (AAC; Solanyl flexibility component), based on butandiol, adipic acid and terephthalic acid, supplied by Rodenburg Company, Netherlands, is used in this study, it has been used and described in previous work.[20] Two grades of linear AAC, AAC1 and AAC2, were used in this work. The shape of polymer as received is spherical granule resin of 3–5 mm in diameter and density of 1.2 g/cm^3 at 25°C. Using differential scanning calorimetry (DSC), the range of melting temperatures is 110–115 °C.

Melt spinning

Fibers were extruded via melt spinning on a Lab-spin machine, Extrusion Systems Limited, UK. The Lab-spin machine has been described in previous study.[20] The molten polymer is forced through the spinneret (55 holes, 0.4 mm) as fine jets with speed adjusted by the metering pump (fixed at 4 rpm) which generates the high pressure during metering. The air cooling quench percentage was set at 37%. The filaments then cool down and solidified progressively to emerge as yarn. The spin finish (0.4 rpm) was diluted five folds with water before use. The filaments were collected from machine rollers set at 36 m/min without tension between them and the winder.

Factorial experimental design

The extrusion experiments conducted involves four factors at two levels as given in Table I, the selection of levels for all variables were being based on a prior screening done as pre-lab work (unpublished data). The selected level range is small to delete any nonlinearity if some factors are related to quality characteristic in a nonlinear way. These selected control factors include the polymer grade described as MFI and the extruder temperature zones. As shown in previous paper[20] and for simplicity, every two consecutive zones are combined and considered as one, i.e. $Z1 = T1 + T2$, $Z2 = T3 + T4$ and $Z3 = T5 + T6$, where the temperatures of barrel zones are $T1$, $T2$ and $T3$, metering pump zone is $T4$ and die head zones are $T5$ and $T6$. The experiments were conducted in two blocks for the polymer grade (MFI) because of the difficulty of cleaning the machine after each run. As a result, the block effect is included in MFI effect.

Interferometric technique

According to the strong relationship between birefringence and molecular orientation,[27] low birefringence fibers have low orientation and would be more draw-able than the higher values and visa versa.

In this work, the subtractive position is applied to give the nonduplicated images for the direct measurement of the fiber's birefringence (Δn) and fiber birefringence was measured using a polarizing interference microscope. The double refracting polarizing interference (Pluta) microscope was designed, developed and applied by Pluta.[28] For accurate and less time consuming measurements, this Pluta microscope was equipped with a computerized unit consisting of a CCD Camera and PC computer. Using this unit the microinterferograms can be captured then automatically analyzed.[29] The birefringence (Δn) of the fiber can be determined indirectly by calculating the difference between the refractive indices ($n^{\parallel} - n^{\perp}$) of the fiber. Here $n^{\parallel}$ and $n^{\perp}$ are the refractive indices of fiber in case of the light polarizing

TABLE I
Factors and Their Levels for the Experiments

	Factor						
	Z1		Z2		Z3		
Level	T1	T2	T3	T4	T5	T6	MFI
−1 (Low)	110	115	120	125	130	130	MFI 1
1 (High)	115	120	125	130	145	145	MFI 2

parallel and perpendicular to the fiber axis, respectively. But it can be measured directly using the subtractive mode of Pluta microscope via the following eq. (1)[30]:

$$\Delta n = \frac{Z\lambda}{bt} \tag{1}$$

Where Z is the fringe shift from the zero-order fringe, λ is the wavelength of the light used, b is the interfringe spacing and t is the fiber diameter. The error of measuring the optical path difference ($Z\lambda/b$) using the interference Pluta microscope ranges from ± 0.001 to ± 0.003.[31]

Differential scanning calorimetry characterization

METTLER-TA Instrument DSC12E and METTLER–TOLEDO–TA89E System Software[32,33] were used to determine the thermal curves of AAC polymer and fiber. The gas used was nitrogen. Average of three replicates scanned for each sample was considered.

Melt flow index

Ray-Ran 5 Series Advanced Melt Flow Systems according to ASTM D-1238 was used to measure the MFI. The instrument contains of a barrel with a standard die and piston. Granules of AAC are loaded into a heater block and left for 10 min to melt (ASTM D-1238) and condition to the right temperature. A fixed pressure was applied to the melt via a piston and different loads of total mass of 2.16, 3.16, 5.00 kg at different temperatures of 120, 125, 130, 135°C. As the piston diameter (D) is bigger than the capillary diameter (d) and the pressure dropped along the capillary (ΔP), the wall shear stress (τ) in the capillary, $\tau = \frac{\Delta P\, d}{4L}$, can be related to the force on the piston, and the entrance effects are neglected,[34] ΔP can be calculated by using the equation $\Delta P = \frac{4F}{\pi D^2}$. The shear stress at the capillary wall is determined by eq. (2):

$$\tau = \frac{Fd}{\pi L D^2} = 8.97\, F \tag{2}$$

Where F is the weight on the plunger in grams, l is the capillary length.

The apparent shear rate at the capillary wall can now be expressed as a function of the MFI[35] by eq. (3):

$$\gamma_{app} = 1.845\, \upsilon \tag{3}$$

The flow rate (υ, cm^3/s) is determined by the area (cm^2) and the piston velocity (v, cm/s) or by the MFI value and the melt density at the current temperature (ρ_t)[35]:

$$\upsilon = \frac{\text{MFI}}{600 \times \rho_t} \tag{4}$$

The apparent viscosity can be determined by dividing the shear stress by the apparent shear rate[35] as shown in eq. (5):

$$\eta_{app} = \frac{4.86\, F}{\upsilon} \tag{5}$$

RESULTS AND DISCUSSION

Rheology of polymers

Two grades of linear AAC, AAC1 and AAC2, were used in this work (Fig. 1). They are coded as MFI1 and MFI2 depending on their MFI. Figure 1 shows the temperature dependant of MFI for the two samples studied. Within a considerable range of melting temperature (120–135°C), the difference between MFI2 and MFI1 increased as the temperature increases. According to DSC results (Fig. 2), the polymer did not melt completely below 120°C but an optimum temperature window was found to take all factors into account, the large peak around −30°C in AAC2 is related to the moisture content. The overall thermal behavior of the polymer used in this work allows the conclusion that the processing temperature window is slightly wide. The multiple melting phenomenon observed could be attributed to compositional heterogeneity of the copolyester, based on this fact, it can be confirmed that AAC is a mixture composed of a number of components with different melting points.

In terms of extrudate surface analysis, smooth extrudate can be observed above 130°C and 'shark skin' extrudate between 125 and 130°C. 'Shark skin' surface was formed by a series of ridges aligned perpendicular to the flow direction and it was distinguished from an elastic turbulence, which belong to the material nature and sometime to the polymer-die

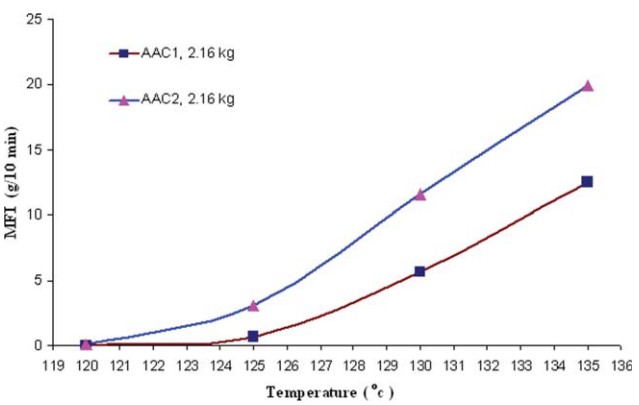

Figure 1 The relationship between MFI and temperature at weight = 2.16 kg. [Color figure can be viewed in the online issue, which is available at www.interscience.wiley.com.]

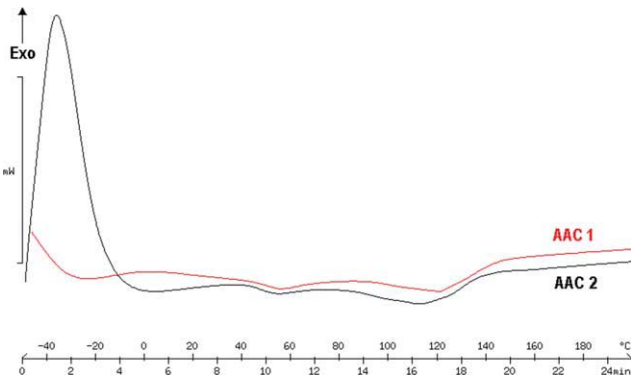

Figure 2 DSC thermographs of AAC fibers. [Color figure can be viewed in the online issue, which is available at www.interscience.wiley.com.]

metal adhesion.[36] Stick-slip or oscillating melt extrudate appears at 125°C, and gross melt fractured extrudate was found at 120°C. It can be seen at lower extrusion rate and it depends on the temperature as shown before. The apparent extrudate swell depends on the die entry and the die exit and possible slip at the polymer-wall interface.[37]

Figures 3 and 4 show the extrudates' appearance at different temperature, apparent shear rate and viscosity related. Melt instability can be caused by excusive increase in shear stress and stick-slip or shark-skin effect will appear. At higher temperature the viscosity was decreased and the material flows easily. At shear rate more than 5 s^{-1}, the extrudate surface was practically smooth and quite smooth up to 15 s^{-1}, whereas smoother extrudates were obtained at shear rate more than 15 s^{-1}. In conclusion, the decrease in viscosity improves the material flow and lead to more uniform extrudate (filaments), hence additional information about the processing window can be obtained.

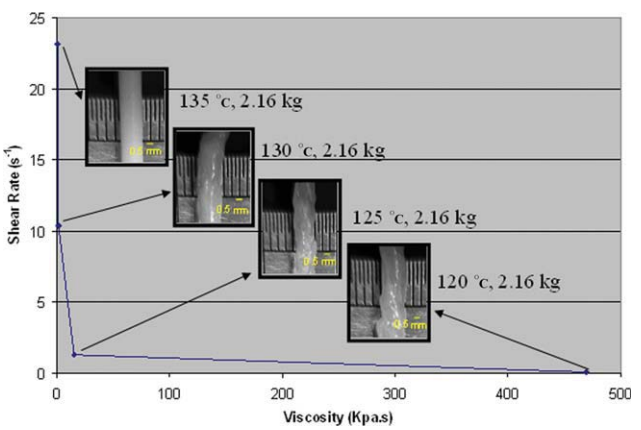

Figure 3 The surface shape at different temperature, viscosity, and shear rate at load of 2.16 kg for AAC1. [Color figure can be viewed in the online issue, which is available at www.interscience.wiley.com.]

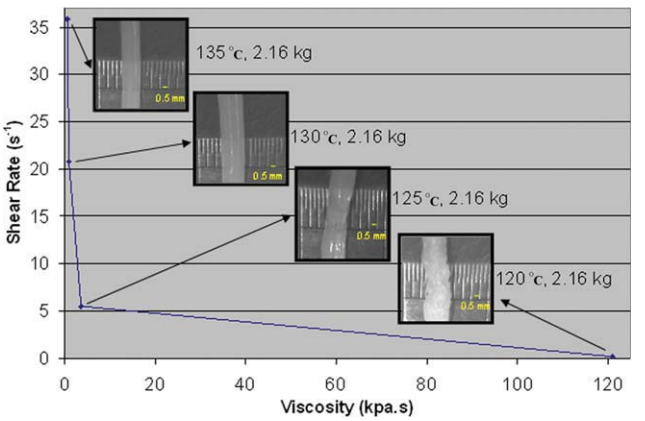

Figure 4 The surface shape at different temperature, viscosity, and shear rate at load of 2.16 kg for AAC2. [Color figure can be viewed in the online issue, which is available at www.interscience.wiley.com.]

Fibers extrusion and modeling

A fraction factorial experimental design was used to design **L16** matrix with random order for sixteen screening trials.[38,39] It is a good practice to randomize the order of the performed design because many things can be changed from production run to another. The detailed experimental arrangement of sixteen trials randomly was given in Table II. Figure 5 show the recorded microinterferograms of fibers using the polarizing (Pluta) microscope using light of wavelength ($\lambda = 550$ nm). It can be seen that the average birefringence has small standard deviations for some reasons such as: (i) blocked nozzles in the spinneret because of the nature of this polymer and the nonuniform flow which decreases at high temperature, (ii) tension during the spinning or (iii) some tension during preparing the sample for the test, (iv) some difference in cooling rate through the

TABLE II
Experimental Array and Results

Trial number	Block	MFI	Z1	Z2	Z3	Birefringence × 10^{-3}
1	1	−1	1	1	1	38.0
2	1	−1	−1	−1	1	22.0
3	2	1	1	−1	1	3.7
4	2	1	1	1	−1	21.7
5	1	−1	1	−1	−1	43.0
6	2	1	−1	−1	−1	22.1
7	1	−1	−1	1	−1	39.0
8	2	1	−1	1	1	0.0
9	1	−1	1	−1	1	19.0
10	2	1	1	1	1	3.0
11	2	1	−1	−1	1	9.3
12	1	−1	−1	−1	−1	44.0
13	2	1	1	−1	−1	17.1
14	2	1	−1	1	−1	10.5
15	1	−1	−1	1	1	28.0
16	1	−1	1	1	−1	38.0

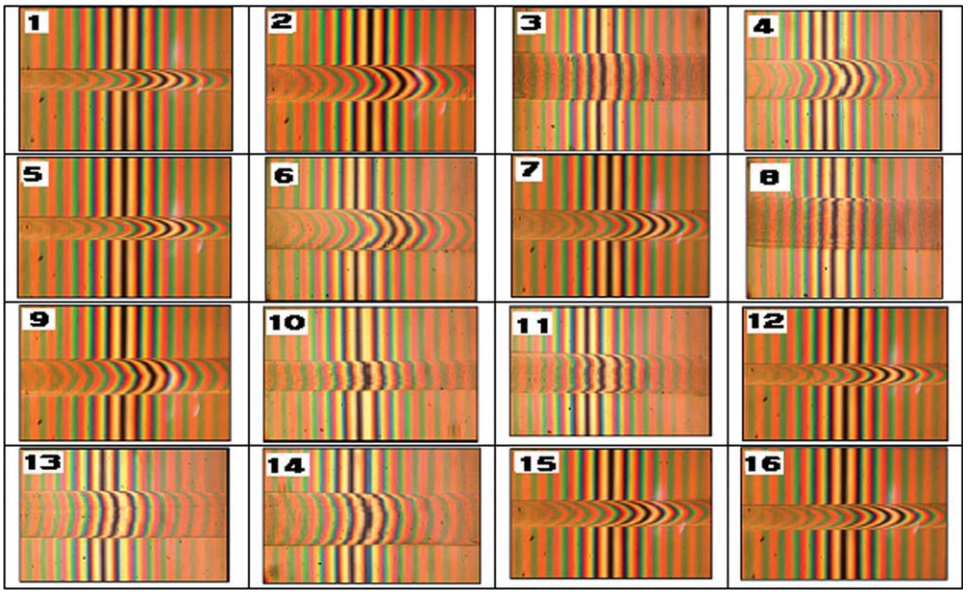

Figure 5 Microinterferograms of birefringence using Pluta microscope. [Color figure can be viewed in the online issue, which is available at www.interscience.wiley.com.]

filaments bundle. The results of the first set of fibers (MFI1)show more birefringent, overall orientation and consistentthan those of the second set (MFI2).

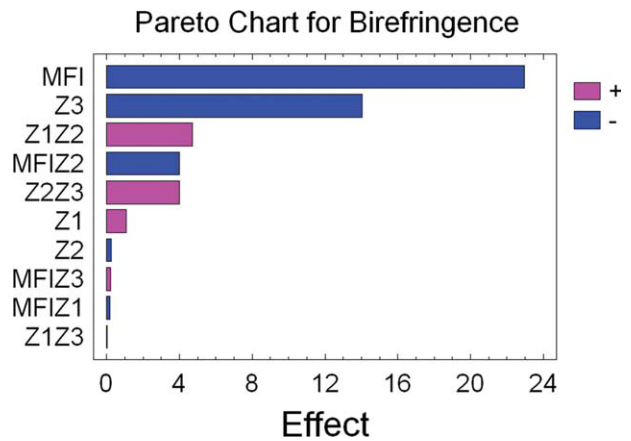

Figure 6 Pareto chart for Birefringence. [Color figure can be viewed in the online issue, which is available at www.interscience.wiley.com.]

Statistical analysis of the effects of the temperature on the overall orientation

A Pareto chart, Figure 6, shows the factors' significant arrangement of factors and their interactions in decreasing order (*y*-axis) depending the significant effect (*x*-axis).

As two-level experiment, a factor effect and interaction effect could be determined as the deference between the average responses at the low and the high level of the factors, the effect line determines the effect of the factors. The longer the effect line the more significant the factor effect, the direction of the effect determine by the slope of the line, i.e., MFI has negative effect as it decreases from left to right. Figure 7 shows the effect plots of the statistical analysis of the effects caused by the main factors and their interactions on the birefringence. All plots are constructed directly from the raw data using STATGRAPHICS and MINITAB programs.[40,41] From these figures (Figs. 6 and 7) it is obvious that, die head

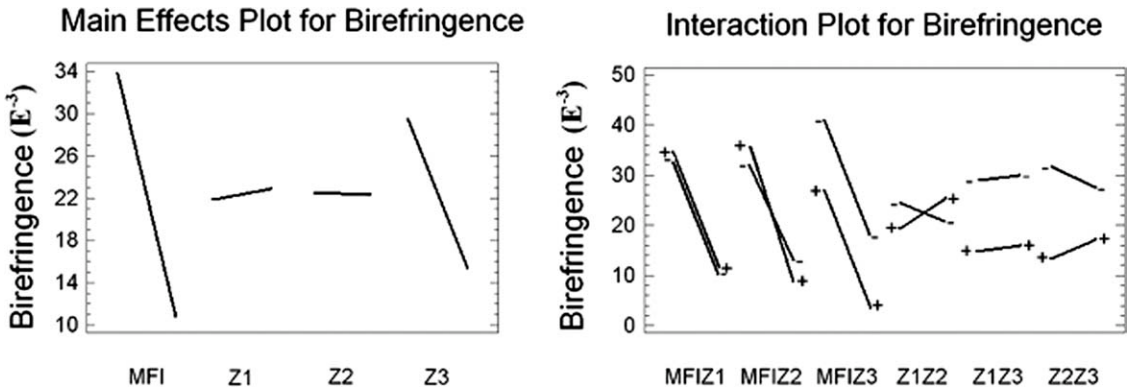

Figure 7 Effect plots and the interaction plots for the response.

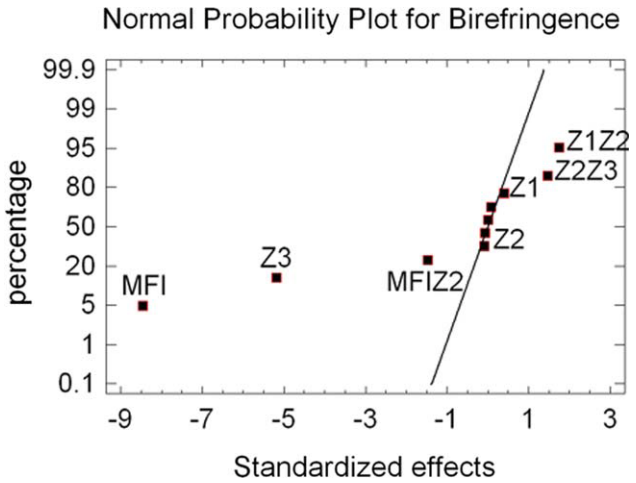

Figure 8 Normal probability plots for the responses. [Color figure can be viewed in the online issue, which is available at www.interscience.wiley.com.]

temperature *Z*3 (*T*5 and *T*6) and the polymer grade (MFI) exert the most significant effects on the overall orientation of fibers. The other main factors, *Z*1 and *Z*2, exhibit little prominence. The interaction noted between *Z*1 and *Z*2 will be discussed separately below to find the significance that may arise from the usual experimental error. The other interactions show no significant interaction effect because of the parallel between some lines in the interaction plots and the very small interaction angle in the others.

As an alternative to an effects plot, a Daniel's plot or normal probability plot can be used to assess the significance of the factors effects,[42] normal probability plot shows the normal distribution of measurements. According to that, the measurement response should follow a normal distribution pattern, if there are no statically significant factors effects in the experiment. The significant effect for both positive and negative effect could be reflected in deviation of the data points from the straight line. The further the deviation, the greater the statistical significance. Figure 8 displays the normal probability (Daniel's) plots and shows the percentage and standardized effects. The effect from MFI and *Z*3 are again prominent. Other factors effect and interactions effect agree with last results, more details can be obtained from analysis of variance.

Analysis of variance for birefringence

Analysis of variance (ANOVA) of the birefringence data was conducted to determine the factor effects in terms of statistical significance.[42] An ANOVA results are listed in Table III. To provide quantitative and objective criteria for judging the statistical significance of the effects, *P*-values of *Z*3 and MFI are less than 0.05 indicating that MFI and *Z*3 are significantly different from zero at the 95.0% confidence

TABLE III
ANOVA Results Identifying the Statistical Significance of Factors Effects

Source	Sum of squares	Df	Mean square	*F*-ratio	*P*-value
MFI	2106.81	1	2106.81	71.61	0.0004
Z1	4.62	1	4.62	0.16	0.7082
Z2	0.25	1	0.25	0.01	0.9301
Z3	789.61	1	789.61	26.84	0.0035
MFI Z1	0.12	1	0.12	0.00	0.9511
MFI Z2	64.0	1	64.0	2.18	0.2002
MFI Z3	0.16	1	0.16	0.01	0.9441
Z1Z2	89.30	1	89.30	3.04	0.1419
Z1Z3	0.003	1	0.003	0.00	0.9930
Z2Z3	64.0	1	64.0	2.18	0.2002
Total error	147.1	5		29.42	
Total (corr.)	3265.98			15	

Df, degree of freedom.

P-value is the smallest risk level α at which the data are significant. F (1, 15) = 4.54 at α = 0.05 under the conditions.

level, *P*-values of *Z*1, *Z*2 and all interactions are greater than 0.05, thus are not significant. The quantitative ANOVA results are consistent with quantitative conclusions derived from the effects plots and Daniel's plots. Figure 9 shows 3D plots of the estimated effects for the high and low settings of three factors *Z*1, *Z*3 and MFI at *Z*2 = 0. As there was no significant interactions have been found, Figure 10 shows estimated response surface plots (3D-surface response diagrams) for interactions *Z*1 and Z2, *Z*2 and *Z*3, and MFI and *Z*2. Estimated response surface plots show no significant twist and no significant effect as a result of these interactions.

The regression equation and estimation results for birefringence

Based on the analysis, the simplified model was fitted by the regression equation [eq. (6)], which has been fitted to the data. The birefringence regression equation in terms of the constant values which

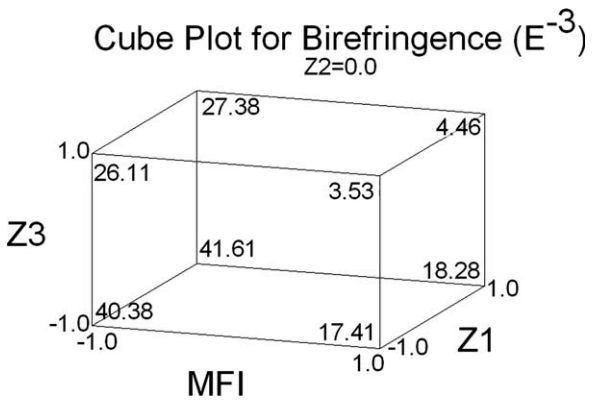

Figure 9 Cube plots of the estimated effects for the high and low settings of three factors.

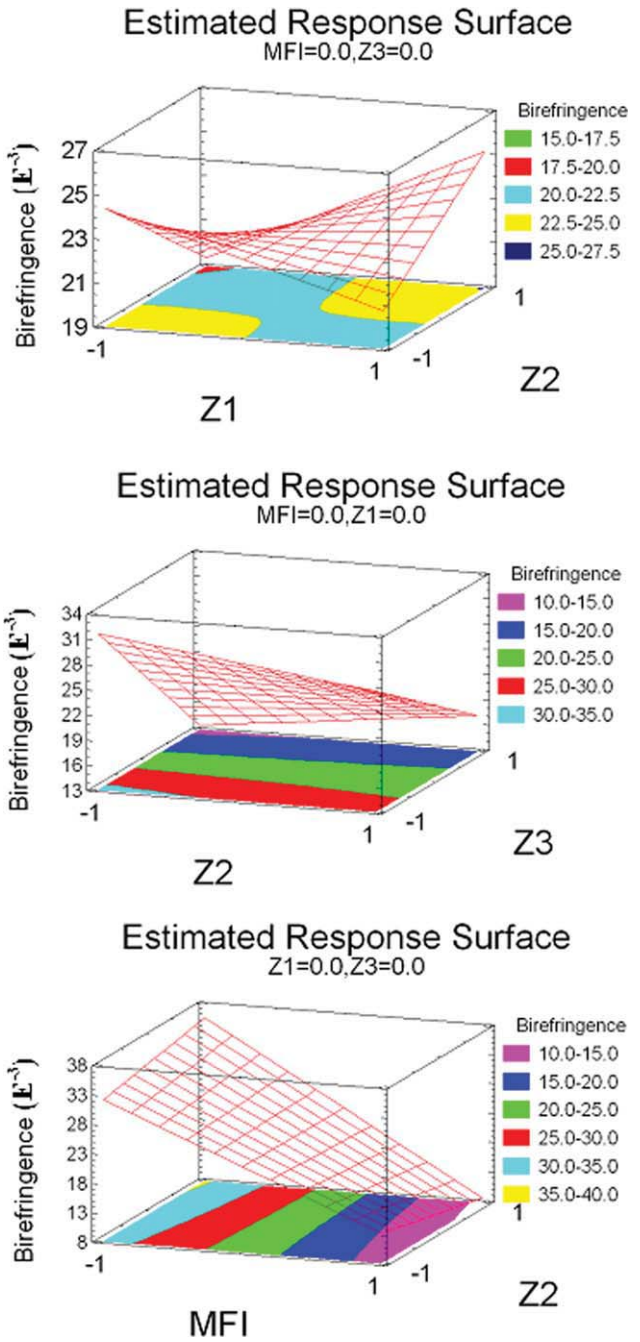

Figure 10 Estimated response surface Z1 and Z2, Z2 and Z3, and MFI and Z2. [Color figure can be viewed in the online issue, which is available at www.interscience.wiley.com.]

includes all interaction terms regardless of their significance is the following:

$$\Delta\mathbf{n}(10^{-3}) = 22.4 - 11.475 \cdot \mathrm{MFI} + 0.5375 \cdot Z1 - 0.125 \cdot Z2 - 7.025 \cdot Z3 - 0.0875 \cdot \mathrm{MFI} \cdot Z1 - 2.0 \cdot \mathrm{MFI} \cdot Z2 + 0.1 \cdot \mathrm{MFI} \cdot Z3 + 2.3625 \cdot Z1 \cdot Z2 + 0.0125 \cdot Z1 \cdot Z3 + 2.0 \cdot Z2 \cdot Z3 \quad (6)$$

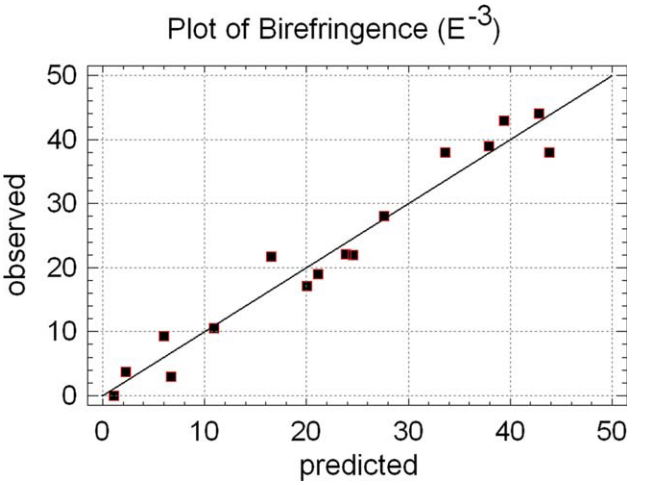

Figure 11 Observed and fitted results for birefringence. [Color figure can be viewed in the online issue, which is available at www.interscience.wiley.com.]

This regression equation is a sufficient basis for interpretation of the obtained relationships $\Delta n = f$ (Z1, Z2, Z3, MFI). Using the last fitted models for each trial, Figure 11 shows that the predicated (fitted) values match observed (experimentally measured) values reasonably.

CONCLUSIONS

In the course of birefringence optimization, the mathematical statistical model was derived from the experimental data and residual plots which were analyzed to validate the regression model. Table IV shows the combination of factor levels which maximize the birefringence over the indicated region, where the optimum (maximum) birefringence value will be 0.0439. The table summarizes the main conclusion of birefringence results in a concise statistical model. The value of the birefringence reflects the overall orientation or the alignment of the molecules along the fiber axis. The suggested model covers both of the identified significant main and interaction factors and specifies the combinations of factor

TABLE IV
The Combination of Factor Levels

Optimum value	Maximum	Minimum
	0.0439	0.0011

The combination of factor levels (Birefringence)				
Factor	Optimum model	Actual value	Optimum model	Actual value
MFI	Low level	MFI1	High level	MFI2
Z1	High level	115–120	Low level	110–115
Z2	High level	125–130	High level	125–130
Z3	Low level	130–130	High level	145–145

levels for enhancing birefringence and therefore the overall orientation of as spun AAC fibers. The obtained fibers can be used as the total fiber content in the fabric in agricultural and horticultural applications such as seed mats, erosions and seasonal weed control ground covers and other nontraditional fibers and fabric applications. In term of extrusion temperature profile, the obtained results implied that the effect of each variable is in agreement with the that previously reported by the authors.[20]

References

1. Steinbüchel, A. Biopolymers; Wiley-VCH: Germany, 2003; Vol. 10.
2. Kang, H. J.; Park, S. S. J Appl Polym Sci 1999, 72, 593.
3. Park, S. S.; Chae, S. H.; Im, S. S. J Polym Sci Part A: Polym Chem 1998, 36, 147.
4. Park, S. S.; Kang, H. J. Polym J 1999, 31, 238.
5. Hayes, R. A. U.S. Pat. 6485819 (2002).
6. Hoppens, N. C.; Hudnall, T. W.; Foster, A.; Booth, C. J. J Polym Sci Part A: Polym Chem 2004, 42, 3473.
7. Twarowska-Schmidt, K. Fibre Text East Eur 2004, 12, 15.
8. Eastman Polymers for Fibres; Eastman chemical company: USA, 2002.
9. Environment Australia, Biodegradable Plastics-Developments and Environmental Impacts, Ref: 3111-01, NOLAN-ITU Pty Ltd, 2002.
10. Witt, U.; Muller, R.-J.; Deckwer, W.-D. J Polym Environ 1995, 3, 215.
11. Fang, Q.; Hanna, M. A. Bioresour Technol 2001, 78, 115.
12. Bastioli, C. Hand Book of Biodegradable Polymers; Rabra Technology: Italy, 2005.
13. Stevens, E. S. Green Plastics, Plastics and the Environment; Princeton University Press: USA, 2001.
14. Fumin, L.; Haile, W. A.; Tincher, M. E.; Harris, W. S. Eur. Pat. EP1330350 (2003).
15. Wang, J. H.; Aimin, H. The World Intellectual Property Organization, Wipo Patent WO/2008/008068 (2008).
16. Lu, F.; Ahaile, W.; Etincher, M.; Wiley, S. H. The World Intellectual Property Organization, Wipo Patent WO/2002/028626 (2002).
17. Twarowska-Schmidt, K.; Ratajska, M. Fibres Text East Eur 2005, 13, 71.
18. Wang, L.; Xie, Z.; Bi, X.; Wang, X.; Zhang, A.; Chen, Z.; Zhou, J.; Feng, Z. Polym Degrad Stab 2006, 91, 2220.
19. Capasso, V. Mathematical Modelling for Polymer Processing; Springer-Verlag: New York, 2003.
20. Younes, B.; Fotheringham, A.; El-Dessouky, H. M. Polym Eng Sci 2009, 49, 2492.
21. Aarts, A. C. T. PhD Thesis, Eindhoven University of Technology, Eindhoven, The Netherlands, 1997.
22. Kadolph, S. J.; Langford, A. L. Textiles; Pearson Education Inc. USA, 2002.
23. Brody, H. Synthetic Fibre Materials; Longman Group UK limited: London, 1994.
24. Ziabicki, A. Fundamental of Fibre Formation; John Wiley & Sons: London, 1976.
25. El-Dessouky, H. M.; Mahmoudi, M. R.; Lawrence, C. A.; Yassien, K. M.; Sokkar, T. Z. N.; Hamza, A. A. Polym Eng Sci 2009, 49, 2116.
26. Giles, H. F.; Wagner, J. R.; Mount, E. M. Extrusion: The Definition Processing Guide and Hand Book; William Andrew Inc. Norwich, 2005.
27. Hermans, H. Contribution to the Physics of Cellulose Fibres; Elsevier: Amsterdam, 1946.
28. Pluta, M. J Microscopy 1971, 93, 83.
29. Sokkar, T. Z. N.; El-Dessouky, H. M.; Shams-Eldin, M. A.; El-Morsy, M. A. Opt Laser Eng 2007, 45, 431.
30. Simmens, S. C. Nature 1958, 181, 1260.
31. Pluta, M. Advanced Light Microscopy: Measuring Techniques; PWN-Polish Scientific Publishers: Warsaw, Poland, 1993.
32. METTLER System software TA89E; METTLER-Toledo AG: Switzerland, 1990.
33. METTLER TOLEDO TA89E System software VERSION 3; METTELER-Toledo AG: Switzerland, 1993.
34. Han, C. D. Rheology in Polymer Processing; Academic Press: New York, 1976.
35. Rawendaal, C. Polymer Extrusion; Hanser: Munich, 2001.
36. Brydson, J. A. Flow Properties of Polymer Melts; George Godwin Limited: London, 1981.
37. Barnes, H. A.; Hutton, J. F.; Walters, K. An Introduction to Rheology; Elsevier Science Publisher: The Netherlands, 1989.
38. Lochner, R. H.; Mater, J. E. Design for Quality; Chapman and Hall: London, 1990.
39. Phadke, M. S. Quality Engineering Using Robust Design; AT&T Bell Laboratories: USA, 1989.
40. STATGRAPHICS. STATGRAPHICS Plus Version 5.1; STATGRAPHICS: USA, 2001.
41. Minitab Inc, MINITAB; Minitab Inc.: USA, 1994.
42. Gardiner, W. P.; Gettinby, G. Experimental Design Techniques in Statistical Practice, A Practical Software-Based Approach; Horwood Publishing Limited: England, 1998.